Int J Comput Vis (2009) 83: 101–119
DOI 10.1007/s11263-009-0221-5

Issues About Retinex Theory and Contrast Enhancement

Marcelo Bertalmío · Vicent Caselles · Edoardo Provenzi

Received: 2 June 2008 / Accepted: 28 January 2009 / Published online: 24 February 2009

Abstract We present an interpretation of Land's Retinex theory that we show to be consistent with the original formulation. The proposed model relies on the computation of the expectation value of a suitable random variable weighted with a kernel function, thus the name Kernel-Based Retinex (KBR) for the corresponding algorithm. KBR shares the same intrinsic characteristics of the original Retinex: it can reduce the effect of a color cast and enhance details in low-key images but, since it can only increase pixel intensities, it is not able to enhance over-exposed pictures. Comparing the analytical structure of KBR with that of a recent variational model of color image enhancement, we are able to perform an analysis of the action of KBR on contrast, showing the need to anti-symmetrize its equation in order to produce a two-sided contrast modification, able to enhance both under and over-exposed pictures. The anti-symmetrized KBR equations show clear correspondences with other existing color correction models, in particular ACE, whose relationship with Retinex has always been difficult to clarify. Finally, from an image processing point of view, we mention that both KBR and its antisymmetric version are free from the chromatic noise due to the use of paths in the original Retinex implementation and that they can be suitably approximated in order to reduce their computational complexity from $\mathcal{O}(N^2)$ to $\mathcal{O}(N \log N)$, being N the number of input pixels.

Keywords Retinex · Contrast enhancement · Variational methods · Color image processing

M. Bertalmío · V. Caselles · E. Provenzi (✉)
Departament de Tecnologies de la Informació i les Comunicacions, Universitat Pompeu Fabra, Carrer Tànger, 122-140, 08018 Barcelona, Spain
e-mail: edoardo.provenzi@upf.edu

M. Bertalmío
e-mail: marcelo.bertalmio@upf.edu

V. Caselles
e-mail: vicent.caselles@upf.edu

1 Introduction

The original Retinex theory (Land and McCann 1971) aims at reproducing the sensory response to color stimuli by the Human Visual System (HVS). The model was developed starting from the assumption that actual color sensations are related to the intrinsic reflectance of objects rather than to the radiance values captured by the eyes. Land and McCann were led to postulate this claim after the famous 'Mondrian' experiments (Land 1977, 1983). They proved that the color perception of patches with different reflectance remains distinct even when the spatial illumination is rearranged in such a way that those patches send the same spectral light distribution to an observer. If color perception were only a light acquisition process, then those different patches would be perceived as having the same color; the fact that they are perceived with distinct color implies that some further elaboration is involved in the complicated process of color perception. Land named the model that tries to reproduce this elaboration 'Retinex', as an amalgamation of 'retina' and 'cortex', since he did not know if the perception process takes place only in the retina or also in the brain cortex.

Many variants on the original Retinex implementation have been proposed. Some of them were faithful to the initial construction and significatively improved the performance of Retinex, while some others introduced drastic changes maintaining the same name. This fact, in the authors' opinion, generated confusion about what the actual

Retinex model is. In the Appendix, Sect. A.1, we present a brief overview about the different Retinex formulations that have appeared during the years, commenting on their similarities and differences. To avoid possible misunderstandings, we stress that in this paper we will use the term Retinex only to refer to Land and McCann's model described in Land and McCann (1971), Land (1977).

It is important to stress that the experiments that originated the Retinex theory did not involve digital images: the Mondrian pictures are 'physical' arrangements of color patches and the experiment showed a numerical correspondence between the output Retinex values and the reflectance of the Mondrian patches (McCann et al. 1976). However, as already suggested by Land himself (1977, 1983), besides color vision purposes, Retinex can also be used to enhance digital images. The implicit assumption underlying this application is that Retinex should turn a generic input picture into a more 'natural' one, i.e. an image closer to what a human observer would perceive if she/he were looking at the same scene when the picture was taken. This is a much debated issue that raises up both technical and philosophical issues, e.g. the fact that we use again the HVS to look at the Retinex output and, moreover, this output is shown on a digital screen, thus the psychophysical match between the color sensation induced by Retinex and that corresponding to the real scene are quite difficult to compare. In this paper we do not want to enter in this debate, since our aim is the analysis of the properties of Retinex from the point of view of color image enhancement.

The development of our analysis on Retinex is based on a new interpretation of its original construction. This permits us to propose a new implementation that still complies with Land's postulates and has several advantages with respect to the canonical 'ratio-reset' Retinex operation (Land and McCann 1971; Land 1977). The proposed method relies on the computation of the expectation value of a suitable random variable weighted with a kernel function, thus the name Kernel-Based Retinex (KBR) for the corresponding algorithm.

We prove that KBR and the original implementations share the same intrinsic properties: they can remove undesired color cast and enhance detail visibility in low key images, but they always increase image brightness and are not idempotent, converging to non-natural images characterized by the presence of a great amount of white pixels (Provenzi et al. 2005).

By comparing the KBR implementation of Retinex with the variational model of color image enhancement proposed in Palma-Amestoy et al. (2009), we show that to overcome its limitations KBR must be 'anti-symmetrized', in a sense that will be specified later, so that it can properly enhance both under and over-exposed images. This analysis reveals novel insights about the Retinex action on contrast. Moreover, we comment on the fact that, adding a simple mechanism of attachment to original data, further iterations of the algorithm converge to fixed-point images not corrupted by white pixels.

Finally, we show that a suitable approximation technique permits to reduce the computational complexity of KBR and of its anti-symmetrizations from $O(N^2)$ to $O(N \log N)$, being N the number of input pixels.

Let us describe the plan of the paper. In Sect. 2, we describe the Retinex model and its main qualitative properties. In Sect. 3, based on the main features of Retinex, we describe the Kernel based Retinex which assumes a non-local two point comparison between pixels. Then, in Sect. 4, we compare the KBR model with a variational formulation of contrast enhancement operations. In particular, differently to the variational formulations, KBR is not able to enhance over-exposed images. Then, by anti-symmetrizing the KBR formula, we discuss the contrast enhancement effects of its terms. In particular, we show that the ACE algorithm (Rizzi et al. 2003) coincides with one of the anti-symmetrizations of Retinex. In Sect. 5, we describe the numerical approach used to compute the image enhancement using KBR and display our experiments in Sect. 6. The conclusions are summarized in Sect. 7. Finally, in the Appendix, we include an overview of other Retinex formulations and the proof of a Lemma useful to compute the first variation of the contrast energy functionals of the paper.

2 The Retinex Model of Color Vision and its Application to Digital Images

In this section we recall the definition of the Retinex model and the basic features of the corresponding algorithm when applied to digital images following the classical papers (Land and McCann 1971; Land 1977) and the mathematical description exposed in (Provenzi et al. 2005).

2.1 Correspondence between Retinex Output Values and Scaled Integrated Reflectance in the Mondrian World

In (Land 1977), Land reports on some color perception experiments where the subject is given a colored square of paper under constant 'white' illumination conditions and she/he must find a matching color patch from a scene with different illuminant. The experiments showed that observers matched colored squares with different radiances but having the same *scaled integrated reflectances*. At each wavelength band (Long, Middle or Short) corresponding to the spectral response of one of the three cone pigments, the *integrated reflectance* of a color patch is defined as a fraction: its numerator is the integral of the radiance of the patch over a

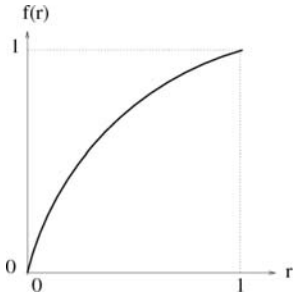

Fig. 1 Non-linear scaling function f. The *horizontal axis* corresponds to (normalized) radiance, while the *vertical axis* corresponds to the sensation of lightness

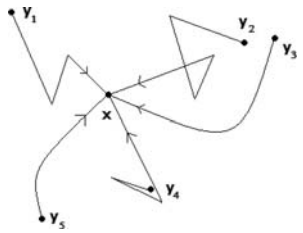

Fig. 2 Five different paths starting in $y_1, \ldots, y_5$ and ending in the target x

given waveband, and its denominator is the integral (over the same band) of the radiance of a white sheet of paper. The *scaling* is given by a non-linear function that relates reflectance with lightness sensation, see Fig. 1.

A photometer measures radiance and would therefore 'match' two surfaces with different reflectance if their radiances were equal, something that can easily be arranged with the correct choice of illuminants (e.g. if two surfaces, each one composed of a distinct uniform reflectance patch covering the entire field of view, were viewed under two lights that make the radiance stimuli match, then they would be judged as identical in color appearance). The HVS, on the other hand, would seem to match patches when their scaled integrated reflectances are equal. Analogous results are given using Mondrian-like figures (Land 1977).

Land wondered how 'the eye' manages to use scale integrated reflectances as an equivalent for lightness 'in the unevenly lighted world without reference sheets of white paper' (Land 1977). The experiments suggested that the eye is able to find the area of maximum lightness ('reference white') and to compare it with areas which may be far away. Land did not think that the eye could directly compare areas which are not next to each other, so he introduced the concept of *sequential product*: in order to compare the radiances $R(x)$ and $R(y)$ at points x and y, respectively, and to compute the fraction $\frac{R(x)}{R(y)}$, we may take any connected path $\gamma = \{z_0, z_1, z_2, \ldots, z_n\}$, a curve that goes from y to x where $z_0 \equiv y$, $z_n \equiv x$, and z_i is the point that follows z_{i-1} on the curve γ. The fraction $\frac{R(x)}{R(y)}$ is just the product of fractions of consecutive points along the path, i.e. $\frac{R(x)}{R(y)} = \frac{R(z_1)}{R(y)} \frac{R(z_2)}{R(z_1)} \frac{R(z_3)}{R(z_2)} \cdots \frac{R(x)}{R(z_{n-1})}$.

Since the HVS is looking for a 'reference white', we must find the point along the path which has maximum radiance. This is equivalent to re-starting the sequential product whenever we reach a point, say z_m, where the radiance is greater than the radiance at any previous point along the path: the sequential product up to z_m is reset to 1, so in practice we re-start by computing $\frac{R(x)}{R(z_m)}$ with the sequential product. The *reset* mechanism is another key element of the Retinex model, as Land (1977) points out:

> 'This [reset] procedure is the heart of the technique for finding the highest reflectance in the path'.

At the end, the sequential product will have the form $\frac{R(x)}{R(z_M)}$, where $R(z_M)$ is the maximum radiance along the path.

The sequential product is scaled with the non-linear function f depicted in Fig. 1. This function may be approximated by Glasser et al.'s (1958) power law, $f(r) = Ar^q + B$, $r \in (0, 1]$, $q \in (0, 1]$, as suggested in McCann et al. (1976), or by a logarithmic function, $f(r) = A' \log(r) + B'$, as in Land (1986), where $r \in [r_0, 1]$ for some $r_0 > 0$ and where A, A', B, B' are real constants. We obtain an estimate for the scaled integrated reflectance and therefore for the lightness $\ell(x)$ at x: $\ell(x) = f(\frac{R(x)}{R(z_M)})$. This estimate has been obtained just for the path γ; to increase the accuracy of lightness estimation N paths are considered, starting at different randomly distributed points y_k, $k = 1, \ldots, N$ but all ending at x (see Fig. 2) and the lightness results obtained for each path are averaged. So, the final Retinex estimate of $\ell(x)$ is:

$$\ell(x) = \frac{1}{N} \sum_{k=1}^{N} f\left(\frac{R(x)}{\max_{z \in \gamma_k}(R(z))} \right), \tag{1}$$

where γ_k is the k-th path used.

This description of the Retinex algorithm does not consider the so-called *threshold mechanism*, a control operation that sets to 1 ratios which differ from 1 by a small amount defined by a threshold. This mechanism was introduced in the original Retinex formulation as a way to reduce the errors produced by noise in the electronic devices of the early 1970's (Land and McCann 1971). During time, it is the authors' belief, the threshold mechanism acquired a misleading role in the model: it was believed that it helped to disregard small gradients due to local illuminant imperfections (Land 1983, p. 5165), however this assumption is not plausible for images more complex than Mondrian-like pictures, because small gradients can also be produced by significant reflectance changes. Nowadays there is a general agreement about the fact that the threshold is a redundant parameter for Retinex, as qualitatively pointed out in McCann (2004), Hurlbert (1986). Moreover, the quantitative analysis performed in Provenzi et al. (2005) about the Retinex formulation that considers the threshold mechanism has shown that, for natural images, the correction given by the threshold mechanism is negligible. For all these reasons, we do not consider the threshold mechanism as an intrinsic element of the Retinex model. Instead, the five steps that we consider as fundamental for the Retinex theory are the following: (i) the

three wavelength bands are dealt with separately; (ii) radiances are compared through ratios; (iii) a reset operation occurs in order to determine the local brightest point; (iv) the ratio-reset output is non-linearly scaled to give a lightness estimation for every fixed path and, finally, (v) the estimations are averaged.

2.2 Application of the Retinex Algorithm to Digital Images

As recalled in the Introduction, we must distinguish between the Retinex theory, which deals with the radiance values of the physical world, and the application of Retinex to digital images, which deals with discrete intensities. In this section we are interested in the analysis of the latter issue.

Let us consider a digital RGB image with spatial domain $\Im = \{1, \ldots, W\} \times \{1, \ldots, H\} \subset \mathbb{Z}^2$, $W, H \geq 1$ being integers; $x = (x_1, x_2)$ and $y = (y_1, y_2)$ denote the coordinates of two arbitrary pixels in $\Im$. We will always consider a normalized dynamic range in $(0, 1]$, so that $\mathbf{I}(x) = (I_R(x), I_G(x), I_B(x))$ is the function representing the *normalized* intensity level of the pixel $x \in \Im$ in the chromatic channels R, G and B, respectively. Notice that we remove the value 0 because the Retinex theory involves ratios, so we have to avoid dividing by zero. For instance, to do that on a 8-bit-per-channel image we just add 1 to each pixel and divide by 256. As already commented, the Retinex theory deals with the three chromatic channels independently, so we will avoid specifying the subindexes R, G and B and we will just write $I(x)$ for the sake of simplicity.

It is worth noticing that, when we take a digital picture, the camera transforms the radiance values that reach its sensors into currents and then into digital intensity values following a particular transformation φ that defines the image formation model of the camera, so that $I(x) = \varphi(R(x))$. Typically φ is a non-decreasing and non-linear function whose precise behavior is difficult to characterize, however popular non-linear image formation models for cameras represents φ as a power-law, i.e. $I(x) = cR(x)^d$, for suitable $c > 0$, $0 < d < 1$, or a logarithmic transformation, i.e. $I(x) = a \log(R(x)) + b$, for suitable values of a, b.

So, taking into account the radiance-to-intensity transformation φ, formula (1) becomes:

$$\ell(x) = \frac{1}{N} \sum_{k=1}^{N} f\left(\frac{\varphi(R(x))}{\max_{z \in \gamma_k}(\varphi(R(z)))} \right)$$

$$= \frac{1}{N} \sum_{k=1}^{N} f\left(\frac{I(x)}{\max_{z \in \gamma_k}(I(z))} \right). \tag{2}$$

In the next subsections, following (Provenzi et al. 2005, 2007), we will use this formula to present two basic properties of the Retinex algorithm and to discuss the role of the paths in the theory.

2.3 The Action of Retinex on Pixel Intensities

Formula (2) has been used in (Provenzi et al. 2005) to easily prove that *Retinex always increases brightness*, i.e. that: $\ell(x) \geq I(x)$, for all $x \in \Im$. Firstly, let's observe that $0 < I(y) \leq 1$ for all $y \in \Im$, so $I(x)/I(y) \geq I(x)$. Secondly, since f is increasing and $f(r) \geq r$, for all $r \in (0, 1]$, we have

$$\ell(x) = \frac{1}{N} \sum_{k=1}^{N} f\left(\frac{I(x)}{\max_{y \in \gamma_k} I(y)} \right)$$

$$\geq \frac{1}{N} \sum_{k=1}^{N} f(I(x)) \geq \frac{1}{N} \sum_{i=1}^{N} I(x) = I(x). \tag{3}$$

This implies that underexposed pictures are usually visibly enhanced by Retinex, while overexposed pictures are not. To overcome this problem, some works introduce a final tone scale correction step in order to guarantee a suitable histogram distribution (Funt et al. 2004).

Another consequence of the lightness formula (2) is that *Retinex is not an idempotent transformation*, i.e. $\ell(\ell(x)) \neq \ell(x)$, in general. The proof of this property is longer than the previous and can be found in Provenzi et al. (2005), where it has been shown that iterating the action of Retinex over and over corresponds to increasing the brightness until the appearance of 'speckling', i.e. white spots spread all over. In Fig. 3 we present an example of such a behavior. If the paths used are short, then the speckling can be so intense that the convergence image may be almost completely white. Of course, neither an image with speckling, nor a white image can be accepted as a plausible convergence result. This property raises up a subtle question: since the action of Retinex on an image continues after the first application and since the convergence image is not acceptable, how many times does Retinex has to be applied on an image to get the best possible enhancement? This remains an open problem strongly

Fig. 3 *Left*: original image. *Right*: convergence image of the Brownian-path Retinex implementation (Marini and Rizzi 2000).

related with subjective judgement. We will see later on that this problem can be handled in the new Retinex implementation that we propose introducing a term that maintains an attachment to original data, see Sect. 5.

2.4 Issues about the Use of Paths: Motivations for Two-Dimensional Retinex Implementations

In (Land 1977), Land wrote:

> 'How can the eye ascertain the reflectance of an area without in effect placing a comparison standard next to the area? The sequential product can be used as a substitute for the placement of two areas adjacent to each other, thus defining a photometric operation feasible for the eye.'

This is a key point. While experiments led Land to conjecture that the eye is in fact comparing areas which are far away, he did not think 'the eye' could perform such an operation directly, so he introduced the paths in the Retinex theory and the computation of sequential products along them. However, as we are going to show, the use of paths in order to extract chromatic information out of an image poses several problems and two-dimensional structures are best suited to this purpose, an objection firstly discussed in Horn (1974) and in Marr (1974) and more recently in Provenzi et al. (2007) by analyzing the consequences of formula (2).

The dependence of the Retinex *implementation* on paths is crucial: if one considers very short paths, then the ratios tend to involve similar values and the resulting image is almost white. On the contrary, if one considers very long paths, then Retinex loses its local nature and reduces to a global White Patch algorithm (each image value is divided by the image maximum, which is assumed to correspond to a white area, hence the name "White Patch") with worse performance (Provenzi et al. 2005). So, paths of 'medium' length have to be considered to obtain good results. Furthermore, a high number of paths must be used ($N \approx 10^1$ or even $N \approx 10^2$, depending on the path geometry adopted) to prevent the formation of sampling noise or artifacts. As we will comment in Sect. A.1, some proposals have been presented in order to optimize path geometry, length and number, however none of them have fulfilled this task.

Paths, being one-dimensional curves in a two-dimensional image, do not really scan local neighborhoods of a point, rather they scan *particular directions* in these neighborhoods. This directional extraction of information can lead to haloes or artifacts in the filtered image. In fact, all the paths of formula (2) end in the same target pixel x, so if x is in a region surrounded by a closed white area, e.g. a white ring, then most paths will intersect the ring and therefore the highest intensity along them will correspond to 1. As a consequence, all points inside the ring will have their values normalized by 1 and so they will remain unchanged, no matter how thin the white ring is: a clear example of this effect in a natural image is the 'dark halo' around the white letters on the book cover of Fig. 5 (left). The classical implementations of Retinex (Land and McCann 1971; Land 1977) try to remedy this problem using a large number of paths, but this increases the filtering time and does not really overcome the problem.

Let us also notice that, for the purpose of lightness computation, two paths ending in the same pixel x may be considered as equivalent whenever they travel the same maximum image value. This permits to organize paths in equivalence classes (Provenzi et al. 2007): in each class one can choose a single representative path to compute lightness, all the other paths in the same class are redundant, in the sense that give exactly the same lightness information.

In the literature there appear approaches that adapt Retinex to use two dimensional neighborhoods instead of paths, see (Horn 1974; Kimmel et al. 2003), however these works lack to consider the reset mechanism, which, as stressed before, is an essential part of the Retinex theory.

The first 2D Retinex implementation faithful to the original Land's theory has been proposed in Provenzi et al. (2007), where paths are replaced by 2-dimensional structures called *random sprays*, which are random sets of samples that lie in a circular area centered in x and with density that decays monotonically as we move away from x, see Fig. 4. This structure is reminiscent of the distribution of cones in the retina, whose density decay as we move far away from the fovea. For random sprays, the decay speed in the distribution of pixels can be easily tuned to fit different purposes; this permits to use them in the approximation of a wide class of algorithms based on local sampling, leading to an appreciable reduction of the filtering time (Provenzi et al. 2008).

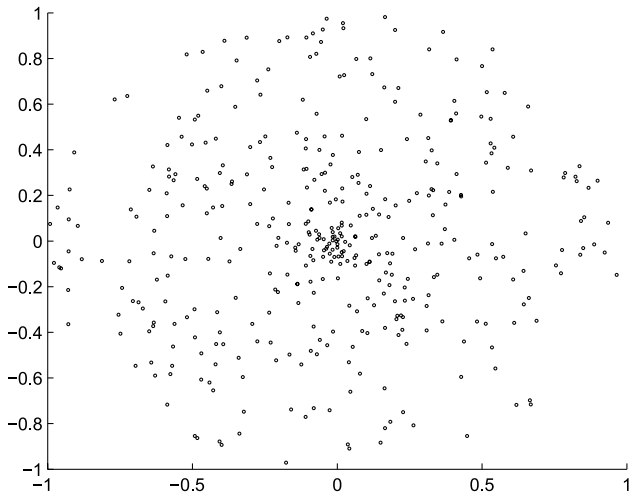

Fig. 4 An example of random spray. Notice that the density sampling is higher close to the center, where the target pixel is placed

Fig. 5 From *left* to *right*: output of Brownian path Retinex and output of RSR, the input image is the picture shown in Fig. 3(left)

To compute the lightness at x using random sprays instead of paths we simply have to center a spray S_x in x, then to search for the brightest pixel inside S_x and, finally, to perform the ratio between $I(x)$ and the highest intensity previously found. If N sprays S_x^k, $k = 1, \ldots, N$ (all centered in x) are used, then the single spray contributions are averaged, giving

$$\ell(x) = \frac{1}{N} \sum_{k=1}^{N} f\left(\frac{I(x)}{\max_{z \in S_x^k} (I(z))} \right), \tag{4}$$

being $I(x) = \varphi(R(x))$ for all $x \in \mathfrak{I}$ as in formula (2). The *Random Spray Retinex* or 'RSR' implementation expressed by (4) is clearly faithful to the original Retinex formulation, the only difference being the fact that the target pixel x is the center of a collection of sprays instead of being the ending point of a set of paths.

The RSR implementation produces outputs with strongly reduced artifacts with respect to the path-wise formulation. In Fig. 5 we compare the output of Brownian path Retinex and RSR; it can be seen that the image filtered with RSR does not show haloes around the white letters, thanks to the fact that it computes the maximum over localized random sets of pixels which are not connected. Yet, some noise may be introduced by RSR in homogeneous zones (Provenzi et al. 2008), and the dependence on spray parameters is still strong and difficult to analyze. Anyway, for what concerns this paper, the most interesting information provided by the RSR implementation is that, even if the path-wise Retinex *implementation* strongly depends on the type of paths used, the Retinex *theory* can be faithfully (and more efficiently) implemented extracting the chromatic information with 2D geometrical structures, without necessarily resorting to paths. We will make use of this information in the next section to propose a novel 2D implementation of Retinex.

3 Kernel-Based Retinex (KBR)

For the sake of clearity, it is worth beginning this section by recalling the basic elements of the Retinex theory, as discussed in Sect. 2: (i) Retinex computations are performed independently for each color channel; (ii) The information carried by the image pixels is compared with ratio operations; (iii) A reset mechanism sets ratios greater than one to a unit value; (iv) The function f of formula (2) performs a non-linear scaling; (v) The scaled ratio-reset comparisons are averaged. Furthermore, from Sect. 2.4 we know that we can avoid the use of paths and perform the ratio comparisons also between non-adjacent pixels, provided that we introduce a weight that decays as the distance between pixels increases, in order to preserve locality.

For convenience, we propose to use the following convention. Given any image $I : \mathfrak{I} \to [0, 1]$ we extend it as an even function with respect to the two variables in the domain $\{-W + 1, \ldots, W\} \times \{-H + 1, \ldots, H\}$ (which we still indicate with $\mathfrak{I}$ for simplicity), i.e. we replicate the image specularly in all directions, and then by periodicity to $\mathbb{Z} \times \mathbb{Z}$ with fundamental period $\mathfrak{I}$. For simplicity, we denote the extended image again by I. With this, we may consider the domain of I as the periodic sampling lattice, that is $\mathbb{T}_d := (\mathbb{Z} \times \mathbb{Z})/(2W\mathbb{Z} \times 2H\mathbb{Z})$. This notation means that we identify any pair of points $x = (x_1, x_2)$ and $y = (y_1, y_2)$ in $\mathbb{Z} \times \mathbb{Z}$ if $x_1 - y_1 \in 2W\mathbb{Z}$ and $x_2 - y_2 \in 2H\mathbb{Z}$. We denote this equivalence relation by $\equiv$. The distance between any two points $x, y \in \mathbb{T}_d$, denoted by $\|x - y\|$, is computed as $\min\{|\tilde{x} - \tilde{y}| : \tilde{x} \equiv x,\ \tilde{y} \equiv y\}$, where $|v| = \sqrt{v_1^2 + v_2^2}$, $v = (v_1, v_2)$. From now on, we shall assume that our images have these symmetry and are defined on the extended domain $\mathfrak{I}$.

Let us then introduce a kernel function, which we require to be a positive, symmetric and normalized weight, i.e. $w : \mathfrak{I} \times \mathfrak{I} \to (0, +\infty)$, $w(x, y) = w(y, x)$ for all $x, y \in \mathfrak{I}$, and

$$\sum_{y \in \mathfrak{I}} w(x, y) = 1, \quad \text{for all } x \in \mathfrak{I}. \tag{5}$$

The kernel $w(x, y)$ represents the probability density of picking a pixel y in the neighborhood of x. In practice this probability is taken as radial and translation invariant, so that $w(x, y) = w(\|x - y\|)$.

We also notice that the reset mechanism and the scaling operation can be merged: in fact, the scaling function f was originally defined as a strictly increasing function $f : (0, 1] \to (0, 1]$ such that $f(r) \geq r$ for all $r \in (0, 1]$, however we can extend f to $(0, +\infty)$ preserving continuity by defining

$$\hat{f}(r) = \begin{cases} f(r) & \text{if } r \in (0, 1] \\ 1 & \text{if } r \in [1, +\infty) \end{cases}.$$

It is clear that applying this new scaling function $\hat{f}$ to the ratios $I(x)/I(y)$, with x fixed and y that varies in $\Im$, jointly implements the scaling and the reset mechanism.

Now we have all the elements we need to define our interpretation of Land's model, which we call Kernel-Based Retinex (KBR from now on). Given $x \in \Im$, let $Y_{w,x}$ be the random variable modeling the selection of a pixel in the neighborhood of x according to the density $w(x, y)$. We define the output $L(x)$ of our algorithm at the pixel x as the conditional expectation of the scaled integrated reflectance $\hat{f}(\frac{I(x)}{I(Y_{w,x})})$ with respect to the distribution w of pixels around x, i.e.

$$L_w(x) = \mathbb{E}_{Y_{w,x}}\left[\hat{f}\left(\frac{I(x)}{I(Y_{w,x})}\right)\right]. \tag{6}$$

This formula is used independently for each color channel and can be written more explicitly as

$$\begin{aligned} L(x) = &\sum_{\{y\in\Im: I(y)\geq I(x)\}} w(x,y) f\left(\frac{I(x)}{I(y)}\right) \\ &+ \sum_{\{y\in\Im: I(y)<I(x)\}} w(x,y). \end{aligned} \tag{7}$$

We stress that all the basic elements of the Retinex theory recalled above are faithfully implemented in (7): the fundamental mechanism of KBR is the propagation of a two-pixel ratio comparison between the fixed target x and the generic pixel y that runs over the entire image; these comparisons are then scaled by $\hat{f}$ and, finally, locally averaged with weight w, in order to produce the value of $L(x)$.

It is useful to rewrite (7) introducing the functions

$$\text{sign}^+(\xi) := \begin{cases} 1 & \text{if } \xi > 0, \\ \frac{1}{2} & \text{if } \xi = 0, \\ 0 & \text{if } \xi < 0, \end{cases} \qquad \text{sign}^-(\xi) = 1 - \text{sign}^+(\xi),$$

then we may rewrite (7) as

$$\begin{aligned} L(x) = &\sum_{y\in\Im} w(x,y) f\left(\frac{I(x)}{I(y)}\right)\text{sign}^+(I(y)-I(x)) \\ &+ \sum_{y\in\Im} w(x,y)\text{sign}^-(I(y)-I(x)). \end{aligned} \tag{8}$$

Notice that the points $y \in \Im$ where $I(y) = I(x)$ are incorporated into the first sum of (7). However, since in that case $f(\frac{I(x)}{I(y)}) = 1$, they could also be incorporated into the second sum of (7), or, equivalently, incorporated in both of them with a multiplicity $\frac{1}{2}$. In consonance with this, we have chosen $\text{sign}^+(0) = \frac{1}{2}$, $\text{sign}^-(0) = \frac{1}{2}$. At this point, this is only a technical issue convenient for later developments.

3.1 The Action of KBR on Pixel Intensities

Let us use (8) to verify that KBR always increases brightness as the original Retinex implementation. Since $f(r) \geq r$ for all $r \in (0, 1]$, then $f(\frac{I(x)}{I(y)}) \geq \frac{I(x)}{I(y)} \geq I(x)$, so

$$\begin{aligned} L(x) \geq &\sum_{y\in\Im} w(x,y) I(x)\text{sign}^+(I(y)-I(x)) \\ &+ \sum_{y\in\Im} w(x,y)\text{sign}^-(I(y)-I(x)) \end{aligned} \tag{9}$$

moreover, being $I(x) \leq 1$, we can write

$$\begin{aligned} L(x) &\geq \sum_{y\in\Im} w(x,y) I(x)\text{sign}^+(I(y)-I(x)) \\ &\quad + \sum_{y\in\Im} w(x,y) I(x)\text{sign}^-(I(y)-I(x)) \\ &= I(x)\sum_{y\in\Im} w(x,y)[\text{sign}^+(I(y)-I(x)) \\ &\quad + \text{sign}^-(I(y)-I(x))] \\ &= I(x)\sum_{y\in\Im} w(x,y) = I(x), \end{aligned} \tag{10}$$

having used the fact that the kernel is normalized. As in the original formulation, this property implies that overexposed pictures could not be enhanced with Retinex unless we use a post-processing stage and that further iterations of Retinex keep on increasing the intensity until a white image is reached.

Thus, the action of KBR on pixel intensities is coherent with that of the original Retinex formulation, as discussed in Sect. 2.3.

3.2 Visual Comparison Between Different Retinex Implementations

To remark the coherence between KBR and the original Retinex theory, let us compare the output results of KBR with those of a path-wise implementation and of RSR. Our purpose here is not to perform a thorough comparison between Retinex implementations, but just to present some visual results to underline the consistency between KBR and Land's theory.

We have selected three different images, each one showing a particular feature and filtered them with the three algorithms. The original images are shown in Fig. 6. From left to right: the first image is characterized by a strong red color cast; the second is a natural image with an upper homogeneous part and a more detailed lower zone; the third is a rather overexposed picture. The outputs of Retinex in the path-wise, RSR and KBR implementations can be found in

Fig. 6 Three original images showing different features

Fig. 7 From *left* to *right*: output of Retinex in the path-wise implementation with Brownian paths (Marini and Rizzi 2000), RSR and KBR

Fig. 8 From *left* to *right*: output of Brownian path Retinex, RSR and KBR

Fig. 9 From *left* to *right*: output of Brownian path Retinex, RSR and KBR

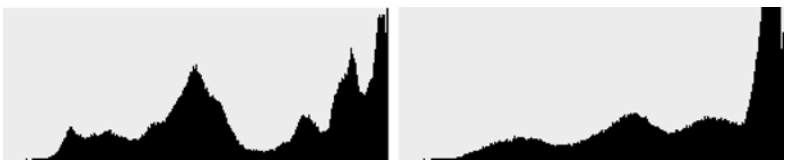

Fig. 10 Histogram of the brightness of the rightmost picture in Fig. 6, before (*left*) and after (*right*) applying Retinex to it. Instead of equalizing the histogram, Retinex produces a non-linear shift towards the white

Figs. 7, 8, 9, respectively. RSR and KBR, sharing the fact of being 2D implementations, show very similar results, while the path-wise Retinex is affected by noise and shows the tendency to increase too much the intensity (as can be noticed looking at the lower part of all three figures). All the implementations can significatively remove color cast and enhance details, except for over-exposed pictures, where, as shown by Fig. 9, they further increase the image brightness. This tendency is clearly shown by the histograms presented in Fig. 10, which refers to the original overexposed image and its filtered version with Brownian path Retinex (the outputs of RSR and KBR have similar histograms).

We consider of basic interest the analysis of this 'one-side enhancement' performed by Retinex, to which is dedicated the next session.

4 Two-Side Contrast Enhancement and KBR

As discussed before, the lightness equations (2), (8) permit to understand the global action of Retinex and KBR, respectively, on pixel intensities. Nonetheless, they do not give any explicit information about the modification of local contrast after the application of Retinex. In this section we show that the contrast change produced by Retinex can be analyzed comparing the KBR equation (8) with that of another color enhancement method discussed in Palma-Amestoy et al. (2009), where a variational framework to perform perceptual color enhancement was introduced and analyzed. Let us briefly recall the features of that variational setting: inspired by the basic phenomenological properties of the HVS, the authors propose a perceptual energy functional $E(I)$ composed by two terms: $E(I) = C_w(I) + D_{I_0,1/2}(I)$,

where $C_w(I)$ is a contrast term, whose minimization produces a *two-sided local contrast enhancement*, locality being induced by the weighting function w; on the contrary, $D_{I_{0,1/2}}(I)$ is a global dispersion term whose minimization controls the dispersion around the input pixel values and around the middle grey, avoiding an excessive departure from the original image and guaranteeing the existence of a non trivial minimum of $E(I)$.

Since we are interested in the investigation of the contrast properties of Retinex, let us fix our attention on the contrast term $C_w(I)$, pointing out how it is capable to deal both with over and under-exposed images without the need of further post-processing stages. For that, let us define an *inverse contrast function* $c(a,b)$ between two intensity levels $a,b>0$ to be a continuous function $c:(0,+\infty)\times(0,+\infty)\to\mathbb{R}$, symmetric in (a,b), i.e. $c(a,b)=c(b,a)$, decreasing when $\min(a,b)$ decreases or $\max(a,b)$ increases, while the other argument remains constant. The most elementary examples of inverse contrast functions are $c(a,b)=-|a-b|\equiv \min(a,b)-\max(a,b)\equiv(\min-\max)(a,b)$ and $c(a,b)=\frac{\min(a,b)}{\max(a,b)}\equiv\frac{\min}{\max}(a,b)$.

As argued in Palma-Amestoy et al. (2009), while the previous assumptions on c are general for any inverse contrast function, if we want c to be able to disregard a global change in intensity, as the HVS does, then we must also require c to be homogeneous. Recall that c is homogeneous of degree $n\in\mathbb{Z}$ if

$$c(\lambda a,\lambda b)=\lambda^n c(a,b)\quad\forall\lambda,a,b\in(0,+\infty), \tag{11}$$

where, in this context, the positive constant λ represents the global change in intensity and a and b represent $I(x)$ and $I(y)$. We can easily see how the homogeneous property affects the intensity change noticing that, since λ can be any positive value, if we set $\lambda=1/b$, we may write equation (11) as:

$$c(a,b)=b^n c\left(\frac{a}{b},1\right)\quad\forall a,b\in(0,+\infty), \tag{12}$$

hence, if c is homogeneous of degree $n=0$, then $b^n=1$, so that c is a function of the ratio a/b and intrinsically disregards the intensity change. Hence, inverse contrast functions $c(I(x),I(y))$ which are homogeneous of degree $n=0$ can be written as $G(\frac{\min}{\max}(I(x),I(y)))$, where $G(r)$ is a monotone non-decreasing function of r. If $n>0$, then the intensity change has a global influence and could be removed performing a suitable normalization (for instance, dividing by the n-th power of the highest intensity level).

Now, assume that w is a positive, normalized and symmetric kernel and $c(a,b)$ is a homogeneous inverse contrast function. Following (Palma-Amestoy et al. 2009), we define the contrast energy functional as

$$C_w(I)=\lambda\sum_{x\in\mathfrak{I}}\sum_{y\in\mathfrak{I}}w(x,y)c(I(x),I(y)), \tag{13}$$

being $\lambda>0$ a suitable normalization constant that will be defined shortly. Since c is an *inverse* contrast function, then the *minimization* of $C_w(I)$ corresponds to a local contrast enhancement for the image I.

To better understand how this takes place, let us consider an explicit homogeneous function of degree 0, such as $c(a,b)=G(\frac{\min}{\max}(I(x),I(y)))$, and calculate the variational derivative of the corresponding contrast energy functional

$$C_w^{\frac{\min}{\max}}(I)\equiv\frac{1}{2}\sum_{x\in\mathfrak{I}}\sum_{y\in\mathfrak{I}}w(x,y)G\left(\frac{\min}{\max}(I(x),I(y))\right). \tag{14}$$

For that we need some technical discussion. Notice that the basic function $t:=\frac{\min(a,b)}{\max(a,b)}$ is not differentiable. In fact, we may write $\min(a,b)=\frac{1}{2}(a+b-|a-b|)$, $\max(a,b)=\frac{1}{2}(a+b+|a-b|)$, for any $a,b\in\mathbb{R}$. The non-differentiability comes from the absolute value $A(z)=|z|$, $z\in\mathbb{R}$. Since our algorithm will use a gradient descent approach, we must regularize the basic variable t. We notice that $A'(z)=1$ if $z>0$, $A'(z)=-1$ if $z<0$ and A is not differentiable at $z=0$. But all the values $s\in[-1,1]$ are *subtangents* of $A(z)$ at $z=0$, that is, $A(z)-A(0)\geq s(z-0)$ for any $z\in\mathbb{R}$. Thus we may write $A'(z)=\operatorname{sign}(z)$, where

$$\operatorname{sign}(z)=\begin{cases}1 & \text{if } z>0\\ [-1,1] & \text{if } z=0\\ -1 & \text{if } z<0\end{cases}. \tag{15}$$

We define $\operatorname{sign}_0(z)$ as in (15), but with the particular choice 0 when $z=0$.

Definition 1 Given $\epsilon>0$, we say that $A_\epsilon(z)$ is a '*nice regularization*' of $A(z)$, if $A_\epsilon(z)\geq 0$ is convex, differentiable with continuous derivative, $A_\epsilon(0)=0$, $A_\epsilon(-z)=A_\epsilon(z)$, and

(i) $A_\epsilon(z)\leq|z|$ for any $z\in\mathbb{R}$ and $A_\epsilon(z)=|z|+Q_{1,\epsilon}(z)$ where $Q_{1,\epsilon}(z)\to 0$ as $\epsilon\to 0$, uniformly in $z\in[-1,1]$;
(ii) Let us denote $s_\epsilon(z)=A'_\epsilon(z)$. Then $|s_\epsilon(z)|\leq 1$ for any $z\in[-1,1]$, $s_\epsilon(z)\to\operatorname{sign}_0(z)$ as $\epsilon\to 0$ for any $z\in\mathbb{R}$, and $Q_{2,\epsilon}(z):=A_\epsilon(z)-zs_\epsilon(z)\to 0$ as $\epsilon\to 0$, uniformly in $z\in[-1,1]$.

We present two examples of nice regularization of $A(z)$. *Example* a): $A_\epsilon(z)=\sqrt{\epsilon^2+|z|^2}-\epsilon$, in this case $s_\epsilon(z)=\frac{z}{\sqrt{\epsilon^2+|z|^2}}$, $Q_{1,\epsilon}(z)=O(\epsilon)$ and $Q_{2,\epsilon}(z):=A_\epsilon(z)-zs_\epsilon(z)=O(\epsilon)$. *Example* b): $A_\epsilon(z)=z\frac{\arctan(z/\epsilon)}{\arctan(1/\epsilon)}-\frac{\epsilon}{2\arctan(1/\epsilon)}\log(1+\frac{z^2}{\epsilon^2})$, in this case $s_\epsilon(z)=\frac{\arctan(z/\epsilon)}{\arctan(1/\epsilon)}$, $Q_{1,\epsilon}(z)=O(\epsilon\log(1/\epsilon))$ and $Q_{2,\epsilon}(z)=O(\epsilon\log(1/\epsilon))$, uniformly in $z\in[-1,1]$. We have denoted by $O(F(\epsilon))$ any expression satisfying $|O(F(\epsilon))|\leq CF(\epsilon)$ for some constant $C>0$ and $\epsilon>0$ small enough. Observe that, in both cases $s_\epsilon(z)\to\operatorname{sign}_0(z)$ as $\epsilon\to 0$ for any $z\in\mathbb{R}$. The proofs of the above statements can be found in Palma-Amestoy et al. (2009).

Now let us assume that $A_\epsilon(z)$ is a nice regularization of $A(z)$. We set

$$\begin{aligned}\min_\epsilon(a,b) &= \frac{1}{2}(a+b-A_\epsilon(a-b)),\\ \max_\epsilon(a,b) &= \frac{1}{2}(a+b+A_\epsilon(a-b)).\end{aligned} \tag{16}$$

We define the regularized version of the functional (14) as:

$$C_{w,\epsilon}^{\frac{\min}{\max}}(I) := \frac{1}{2}\sum_{x\in\mathfrak{I}}\sum_{y\in\mathfrak{I}} w(x,y)G\left(\frac{\min_\epsilon(I(x),I(y))}{\max_\epsilon(I(x),I(y))}\right). \tag{17}$$

Proposition 1 *The first variation of* $C_{w,\epsilon}^{\frac{\min}{\max}}w(I)$ *is*

$$\begin{aligned}\delta C_{w,\epsilon}^{\frac{\min}{\max}}(I) = &-\sum_{y\in\mathfrak{I}} w(x,y)g\left(\frac{I(x)}{I(y)}\right)\\ &\times\frac{I(y)}{\max_\epsilon(I(x),I(y))^2}s_\epsilon(I(x)-I(y))+S'_\epsilon,\end{aligned} \tag{18}$$

where $S'_\epsilon = O(Q_{1,\epsilon}(I(x)-I(y))+Q_{2,\epsilon}(I(x)-I(y)))$ *is a small correction term, and* $g(r)\equiv G'(r)$.

The proof of this result can be found in Palma-Amestoy et al. (2009). It follows easily from the general differentiation Lemma given in the Appendix, Sect. A.2.

When $\epsilon\to 0+$, we obtain $\delta C_w^{\frac{\min}{\max}}(I) := \lim_{\epsilon\to 0+}\delta C_{w,\epsilon}^{\frac{\min}{\max}}(I)$:

$$\begin{aligned}&\delta C_w^{\frac{\min}{\max}}(I)\\ &= -\sum_{y\in\mathfrak{I}} w(x,y)g\left(\frac{I(x)}{I(y)}\right)\\ &\quad\times\frac{I(y)}{\max(I(x),I(y))^2}\operatorname{sign}_0(I(x)-I(y))\\ &= \sum_{y\in\mathfrak{I}} w(x,y)g\left(\frac{I(x)}{I(y)}\right)\frac{1}{I(y)}\operatorname{sign}^+(I(y)-I(x))\\ &\quad-\sum_{y\in\mathfrak{I}} w(x,y)g\left(\frac{I(y)}{I(x)}\right)\frac{I(y)}{I(x)^2}\operatorname{sign}^-(I(y)-I(x)),\end{aligned} \tag{19}$$

Let us now consider a homogeneous function of degree 1 by taking $c(a,b)=(\min-\max)(a,b)$, and

$$\begin{aligned}C_w^{\min-\max}(I) \equiv &\frac{1}{2}\sum_{x\in\mathfrak{I}}\sum_{y\in\mathfrak{I}} w(x,y)(\min(I(x),I(y))\\ &-\max(I(x),I(y))).\end{aligned} \tag{20}$$

In this case we have:

Proposition 2 *Computing the first variation of*

$$\begin{aligned}C_{w,\epsilon}^{\min-\max}(I) \equiv &\frac{1}{2}\sum_{x\in\mathfrak{I}}\sum_{y\in\mathfrak{I}} w(x,y)(\min_\epsilon(I(x),I(y))\\ &-\max_\epsilon(I(x),I(y)))\end{aligned} \tag{21}$$

and letting $\epsilon\to 0+$ *we obtain* $\delta C_w^{\min-\max}(I) := \lim_{\epsilon\to 0+}\delta C_{w,\epsilon}^{\min-\max}(I)$ *given by*

$$\delta C_w^{\min-\max}(I)(x) = \sum_{y\in\mathfrak{I}} w(x,y)\operatorname{sign}_0(I(y)-I(x)). \tag{22}$$

Again, the proof of this result can be found in Palma-Amestoy et al. (2009) and it follows easily from the general differentiation Lemma given in the Appendix, Sect. A.2.

These two examples show the influence of the homogeneity degree on the analytic form of the first variation. In fact, since the derivative of a homogeneous function of degree n is a homogeneous function of degree $n-1$, to restore the homogeneity after the variational derivative we must multiply it by $I(x)^{1-n}$. Obviously, the only trivial case corresponds to the degree 1, such as the case $(\min-\max)(I(x),I(y))$, however, all the functions with a homogeneity degree different from 1 will be correctly normalized, e.g.

$$\begin{aligned}&I(x)\delta C_w^{\frac{\min}{\max}}(I)(x)\\ &= \sum_{y\in\mathfrak{I}} w(x,y)g\left(\frac{I(x)}{I(y)}\right)\frac{I(x)}{I(y)}\operatorname{sign}^+(I(y)-I(x))\\ &\quad-\sum_{y\in\mathfrak{I}} w(x,y)g\left(\frac{I(y)}{I(x)}\right)\frac{I(y)}{I(x)}\operatorname{sign}^-(I(y)-I(x)).\end{aligned} \tag{23}$$

We can now propose the definition of the *variational contrast lightness*. First of all, let the normalization constant λ appearing in (13) be such that $-1\le I(x)^{1-n}\delta C_w(I)(x)\le 1$. Then, since the *minimization* of $C_w(I)$ corresponds to a contrast enhancement and since $-\delta C_w(I)$ gives the fastest decreasing rate of $C_w(I)$, it is natural to define the variational contrast lightness (of homogeneity degree n) as follows

$$\mathcal{L}_n(x) = \frac{1}{2}-\frac{1}{2}I(x)^{1-n}\delta C_w(I)(x)\quad\forall n\in\mathbb{Z}, \tag{24}$$

where $1/2$ is introduced just to assure that $\mathcal{L}_n(x)\in[0,1]$. Notice that if we change the sign of the contrast term from minus to plus, i.e. $\mathcal{L}_n(x)=\frac{1}{2}+\frac{1}{2}I(x)^{1-n}\delta C_w(I)(x)$, the process is inverted and now *contrast is decreased*.

For later purposes, let us highlight the particularly interesting cases corresponding to $n=0,1$:

$$\mathcal{L}_0(x) = \frac{1}{2}-\frac{1}{2}I(x)\delta C_w(I)(x); \tag{25}$$

$$\mathcal{L}_1(x) = \frac{1}{2}-\frac{1}{2}\delta C_w(I)(x). \tag{26}$$

If we substitute the explicit expressions of $\delta C_w^{\frac{\min}{\max}}(I)(x)$ and $\delta C_w^{\min-\max}(I)(x)$ in the formulae relative to $n=0$ and $n=1$, respectively, then we can see that the computation of the lightness is realized through modulations of positive and negative sign around $1/2$. This is precisely what allows the corresponding algorithm to enhance both under and over-exposed images.

We explore this property in more detail in the following subsection, commenting on similarities and differences between the variational contrast lightness formula and those of KBR and another color correction algorithm called ACE (Rizzi et al. 2003).

4.1 Anti-Symmetrization of the KBR Equation

Since the minimization of the functional $C_w(I)$ increases contrast, the gradient descent direction $-I(x)^{1-n}\delta C_w(I)(x)$ goes towards a contrast enhancement. If we compare the KBR Retinex formulation given by (8) with $-I(x)\delta C_w^{\frac{\min}{\max}}(I)(x)$ (see (23)) we can see that there is a fundamental difference in the first term: all pixels y such that $I(y) > I(x)$, give a *positive* contribution to the computation of $L(x)$ in (8), while they give a *negative* contribution to $-I(x)\delta C_w^{\frac{\min}{\max}}(I)(x)$. As noticed above, it is the *antisymmetry* (with respect to the diagobal $I(x)=I(y)$) shown by (23) what permits a two-sided contrast modification able to enhance both overexposed and underexposed images, thus it is interesting to analyze what happens if we anti-symmetrize the analytic expression of (8).

Let us consider two possibilities, either we consider the function $f(\frac{I(x)}{I(y)})\operatorname{sign}^+(I(y)-I(x))$ and we anti-symmetrize it on the region $\{x\in\Im : I(y)\le I(x)\}$, or we consider the function $\operatorname{sign}^-(I(y)-I(x))$ and we anti-symmetrize it on the region $\{x\in\Im : I(y)\ge I(x)\}$.

4.1.1 *Anti-Symmetrization of the First Term of the KBR Equation*

Let us start by analyzing the first case: we want to anti-symmetrize the function

$$\overline{F_1}(I(x),I(y)) \equiv f\left(\frac{I(x)}{I(y)}\right) \quad \text{if } I(x)\le I(y), \tag{27}$$

so we change the overall sign and exchange the position between $I(x)$ and $I(y)$, i.e.

$$\underline{F_1}(I(x),I(y)) \equiv -f\left(\frac{I(y)}{I(x)}\right) \quad \text{if } I(y)\le I(x). \tag{28}$$

Hence, the anti-symmetrized function is $\overline{F_1}(I(x),I(y))$ when $I(x)\le I(y)$ and $\underline{F_1}(I(x),I(y))$ when $I(y)\le I(x)$, i.e.

$$\begin{aligned} F_1(I(x),I(y)) \equiv{}& f\left(\frac{I(x)}{I(y)}\right)\operatorname{sign}^+(I(y)-I(x)) \\ &- f\left(\frac{I(y)}{I(x)}\right)\operatorname{sign}^-(I(y)-I(x)), \end{aligned} \tag{29}$$

which is a homogenous function of degree 0.

Now, if we consider a density field $w(x,y)$ and we take the conditional expectation of the random variable $F_1(I(x),I(Y_{w,x}))$ as in Sect. 3, we have:

$$\begin{aligned} &\mathbb{E}[F_1(I(x),I(Y_{w,x}))] \\ &\quad= \sum_{y\in\Im} w(x,y) f\left(\frac{I(x)}{I(y)}\right)\operatorname{sign}^+(I(y)-I(x)) \\ &\qquad- \sum_{y\in\Im} w(x,y) f\left(\frac{I(y)}{I(x)}\right)\operatorname{sign}^-(I(y)-I(x)). \end{aligned} \tag{30}$$

Notice now that, if we set

$$C_w^{F(\frac{\min}{\max})}(I) \equiv \frac{1}{2}\sum_{x\in\Im}\sum_{y\in\Im} w(x,y) F\left(\frac{\min}{\max}(I(x),I(y))\right), \tag{31}$$

being F the function satisfying the equation $F'(r)r = f(r)$ for all $r\in\mathbb{R}^+$, thanks to Proposition 1 we have that $\mathbb{E}[F_1(I(x),I(Y_{w,x}))] = \delta C_w^{F(\frac{\min}{\max})}(I)(x)$. Thus, if we use as in (6) or, equivalently, (8), the term $\mathbb{E}[F_1(I(x),I(Y_{w,x}))]$ as lightness, then we are indeed decreasing the contrast measured by the functional $C_w^{F(\frac{\min}{\max})}(I)$. The first term in (8) has not the right sign in order to increase contrast. It corresponds to the bilateral filter (Tomasi and Manduchi 1998; Barash 2002), a variational method to reduce the contrast of images in a local non-linear way while respecting edges.

But, on the other hand, since F_1 is homogeneous of degree 0 we can define the associated variational contrast lightness using (25), i.e.

$$\begin{aligned} \mathcal{L}^{F_1}(x) &\equiv \frac{1}{2} - \frac{1}{2} I(x)\mathbb{E}[F_1(I(x),I(Y_{w,x}))] \\ &= \frac{1}{2} - \frac{1}{2} I(x)\delta C_w^{F(\frac{\min}{\max})}(I)(x). \end{aligned} \tag{32}$$

This expression can enhance both under and over-exposed images. To give an explicit example of function F, let us consider the very common case in which f acts as a gamma transformation, i.e. $f(r)=r^\gamma$, for $\gamma\in\mathbb{R}^+$. In this situation the equation that defines F is $F'(r)r = r^\gamma$, whose general solution is $F(r) = \frac{1}{\gamma}r^\gamma + k$, $k\in\mathbb{R}$.

4.1.2 Anti-Symmetrization of the Second Term of the KBR Equation

The anti-symmetrization of the second term in (8)

$$\underline{F_2}(I(x), I(y)) \equiv \text{sign}^-(I(y) - I(x)) \quad \text{if } I(y) \leq I(x), \tag{33}$$

would give the function

$$F_2(I(x), I(y)) \equiv \text{sign}^-(I(y) - I(x)) - \text{sign}^-(I(x) - I(y)). \tag{34}$$

If we consider again a density field $w(x, y)$ and we take the conditional expectation of the random variable $F_2(I(x), I(Y_{w,x}))$, after cancelation of the terms where $I(x) = I(y)$ we have:

$$\mathbb{E}[F_2(I(x), I(Y_{w,x}))] = \sum_{y \in \mathfrak{I}} w(x, y)\, \text{sign}_0(I(x) - I(y)), \tag{35}$$

so, thanks to Proposition 2, we have that $\mathbb{E}[F_2(I(x), I(Y_{w,x}))] = -\delta C_w^{\min-\max}(I)(x)$. This time we observe that the second term in (8) has the right sign to increase contrast, in coincidence with the variational contrast lightness given by

$$\mathcal{L}^{F_2}(x) = \frac{1}{2} - \frac{1}{2}\delta C_w^{\min-\max}(I)(x), \tag{36}$$

since $C_w^{\min-\max}(I)$ is homogeneous of degree 1. Again, this expression can enhance both under and over-exposed images.

This expression corresponds to the equation of an existing method of color correction called ACE (Rizzi et al. 2003). What we have just proven, i.e. that ACE can be seen as a particular anti-symmetrization of the KBR model, gives an answer to the question about which is the link between Retinex and ACE, a problem that has been matter of research in recent years, see e.g. (Palma-Amestoy et al. 2009; Rizzi et al. 2004; Bertalmío et al. 2007).

5 Attachment to Original Data and Convergence of Algorithms

As already proven in Sect. 3.1, KBR is not idempotent. Instead of dealing with the highly subjective task of choosing the optimum number of iterations that should be performed in order to get the best enhancement, we can more efficiently re-write (8) in the form of a Partial Differential Equation (PDE): $I_t(x) = L(x, t) - I(x, t)$, into which we introduce an *attachment to data* term that leaves the image unchanged once it has departed too much from the original:

$$I_t(x,t) = \sum_{y \in \mathfrak{I}} w(x,y)\Big[f\Big(\frac{I(x,t)}{I(y,t)}\Big)\,\text{sign}^+(I(y,t) - I(x,t)) + \text{sign}^-(I(y,t) - I(x,t))\Big] - I(x,t) - \lambda(I(x,t) - I_0(x)), \tag{37}$$

where $\lambda > 0$ weights the strength of the attachment to the original image data $I_0(x) \equiv I(x, 0)$.

Discretizing the derivative and applying a forward-time numerical scheme for this equation we find:

$$I^{k+1}(x) = \Delta t \sum_{y \in \mathfrak{I}} w(x,y)\Big[f\Big(\frac{I^k(x)}{I^k(y)}\Big)\,\text{sign}^+(I^k(y) - I^k(x)) + \text{sign}^-(I^k(y) - I^k(x))\Big] + I^k(x)[1 - \Delta t(1+\lambda)] + \lambda \Delta t I^0(x), \tag{38}$$

where the upper-index $k \in \mathbb{N}$ denotes the iteration number, $I^0(x) \equiv I_0(x)$ is the original image and Δt is the time step.

The anti-symmetrized KBR versions defined by (32) and (36) have a variational formulation, so, in order to construct convergent algorithms, we can add an attachment to data mechanism in the form of a dispersion term in the corresponding energy functionals, as done in Palma-Amestoy et al. (2009). The minimization of this term should control the departure from the middle gray $1/2$ and from the original data value $I_0(x)$, thus providing an opponent mechanism to the contrast enhancement. For that, in principle, every coherent distance function involving $1/2$ and I_0 can be used, however in Palma-Amestoy et al. (2009) it has been shown that the *entropic distance* is the most suitable candidate if one wants to preserve the homogeneity property of the contrast term. The *entropic dispersion* term can be explicitly written as

$$D^{\mathcal{E}}_{\alpha,\beta}(I) := \alpha \sum_{x \in \mathfrak{I}} \Big[\frac{1}{2}\log\frac{1}{2I(x)} - \Big(\frac{1}{2} - I(x)\Big)\Big] + \beta \sum_{x \in \mathfrak{I}} \Big[I_0(x)\log\frac{I_0(x)}{I(x)} - (I_0(x) - I(x))\Big], \tag{39}$$

where $\alpha, \beta > 0$ measure the strength of the attachment to $1/2$ and to $I_0(x)$, respectively.

The total energies of the two anti-symmetrized KBR versions are then:

$$E^{F(\frac{\min}{\max})}_{\alpha,\beta,w}(I) \equiv D^{\mathcal{E}}_{\alpha,\beta}(I) + C_w^{F(\frac{\min}{\max})}(I), \tag{40}$$

and

$$E_{\alpha,\beta,w}^{\min-\max}(I) \equiv D_{\alpha,\beta}^{\mathcal{E}}(I) + C_{w}^{\min-\max}(I). \tag{41}$$

The minimum of a generic energy E satisfies the equation $\delta E(I) = 0$. To search for it we can use a semi-implicit discrete gradient descent strategy with respect to I or every monotonic function of I. For our purposes it is convenient to use $\log I$ in (40), which amounts to using *the relative entropy as a metric* (see Ambrosio et al. 2005). The continuous gradient descent equation is

$$\partial_t \log I(x) = -\delta E(I)(x), \tag{42}$$

being t the evolution parameter. Since $\partial_t \log I = \frac{1}{I}\partial_t I$, we have

$$\partial_t I(x) = -I(x)\delta E(I)(x). \tag{43}$$

As proven in Palma-Amestoy et al. (2009), by discretizing $\partial_t I(x)$ and computing the first variation of the energy, we arrive at this iterative scheme:

$$I^{k+1}(x) = \frac{I^k(x) + \Delta t(\frac{\alpha}{2} + \beta I_0(x) + \frac{1}{2}R_{I^k}^{\text{contr}}(x))}{1 + \Delta t(\alpha + \beta)}, \tag{44}$$

where $k \in \mathbb{N}$ and $R_{I^k}^{\text{contr}}(x)$ varies depending on the contrast term used to define the energy, and it is either

$$\begin{aligned} &R_{I^k}^{F(\frac{\min}{\max})}(x) \\ &\quad\equiv \sum_{y\in\mathfrak{I}} w(x,y) f\left(\frac{I^k(y)}{I^k(x)}\right) \operatorname{sign}^+(I^k(x) - I^k(y)) \\ &\qquad - \sum_{y\in\mathfrak{I}} w(x,y) f\left(\frac{I^k(x)}{I^k(y)}\right) \operatorname{sign}^-(I^k(x) - I^k(y)); \end{aligned} \tag{45}$$

or

$$R_{I^k}^{\min-\max}(x) \equiv \sum_{y\in\mathfrak{I}} w(x,y) \operatorname{sign}_0(I^k(x) - I^k(y)). \tag{46}$$

The proof of the convergence of these methods to a non-trivial fixed point image can be found in Palma-Amestoy et al. (2009). In the next section we will show the results of these algorithms on digital pictures.

Let us finally point out that, by introducing a term of attachment to the original data and writing the KBR equation in the form of a PDE, we end up with a Retinex equation which has the form of a Wilson-Cowan equation, which describes how the activity of a population of neurons in the region $V1$ of the visual cortex evolves in time (Bressloff et al. 2002; Wilson and Cowan 1972, 1973). For more details see (Bertalmío and Cowan 2009). A similar analogy between the Wilson-Cowan equations and the variational formulation of ACE was presented in (Bertalmío et al. 2007).

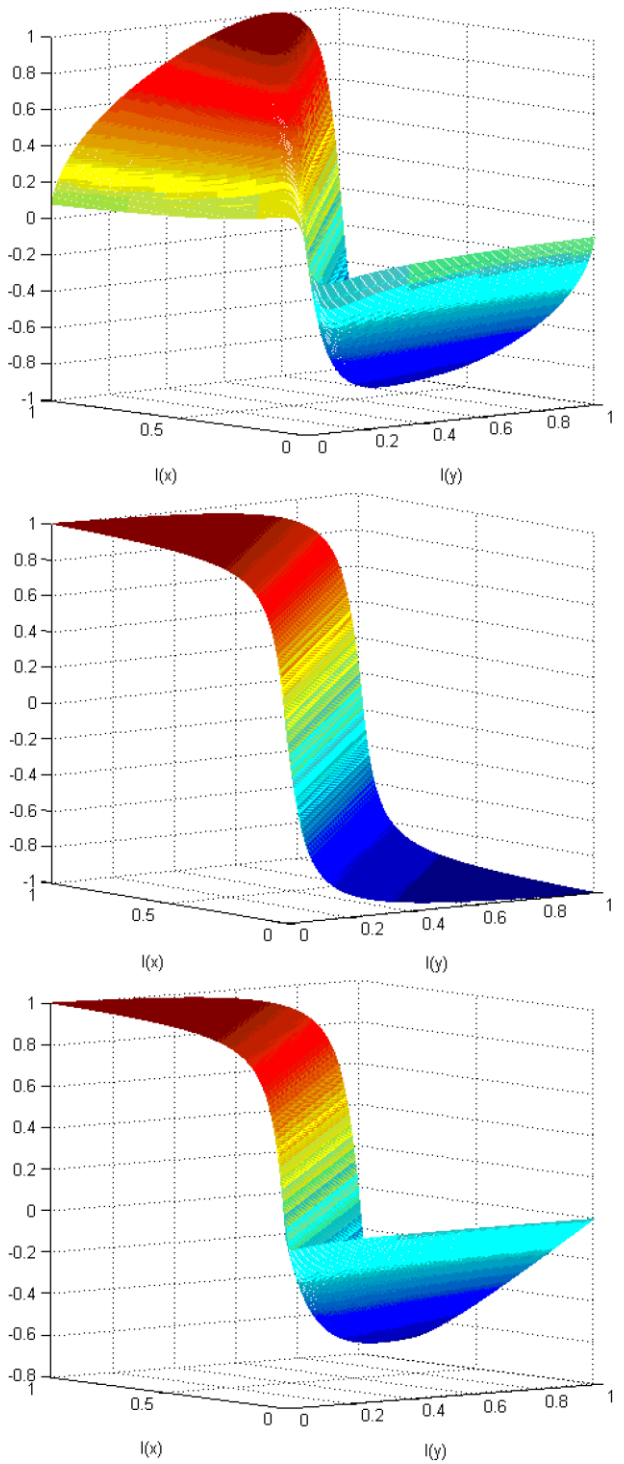

Fig. 11 From *top* to *bottom*: surfaces of $r^{F(\frac{\min}{\max})}$, $r^{\min-\max}$ and r^{KBR} with $\operatorname{sign}(r)$ smoothed by $s_{20}(r)$, the number 20 has been arbitrarily chosen to permit a clear visualization of the surfaces

Remark In each algorithm that we are considering, the contrast modification is represented by a term which has the following form

$$R(x) = \sum_{y\in\mathfrak{I}} w(x,y) r(I(x), I(y)) \tag{47}$$

for suitable functions r, namely

$$r^{F(\frac{\min}{\max})}(I(x), I(y)) \equiv f\left(\frac{I(y)}{I(x)}\right)\text{sign}^+(I(x)-I(y)) - f\left(\frac{I(x)}{I(y)}\right)\text{sign}^-(I(x)-I(y)), \tag{48}$$

for $R_{I^k}^{F(\frac{\min}{\max})}(x)$,

$$r^{\min-\max}(I(x), I(y)) \equiv \text{sign}(I(x)-I(y)), \tag{49}$$

for $R_{I^k}^{\min-\max}(x)$, and

$$r^{\text{KBR}}(I(x), I(y)) \equiv f\left(\frac{I(x)}{I(y)}\right)\text{sign}^+(I(y)-I(x)) + \text{sign}^-(I(y)-I(x)), \tag{50}$$

for

$$R^{\text{KBR}} \equiv \sum_{y\in\mathfrak{I}} w(x,y)\left[f\left(\frac{I(x)}{I(y)}\right)\text{sign}^+(I(y)-I(x)) + \text{sign}^-(I(y)-I(x))\right]. \tag{51}$$

Actually, to avoid abrupt contrast changes, it is more appropriate to consider a smooth approximation of the sign function, as e.g. $s_p(r) \equiv \arctan(pr)/\arctan(p)$, where $p > 1$ controls the slope of the approximating function. For a rigorous analysis of the sign regularization we refer to Palma-Amestoy et al. (2009).

The surfaces representing these functions with smoothed sign are shown in Fig. 11. It can be clearly seen that, while the two r-functions relative to the anti-symmetrized KBR algorithm are balanced at both sides, the one relative to KBR is not, showing hybrid features from both anti-symmetrized surfaces.

6 Experiments

As it has been presented so far, the complexity of KBR and its anti-symmetric versions is the same as the complexity of the original Retinex: $\mathcal{O}(N^2)$, where N is the number of pixels in the image. However, we may use the same technique described in Palma-Amestoy et al. (2009), Bertalmío et al. (2007) to reduce the complexity to $\mathcal{O}(N \log N)$. Since this technique is rather long to explain and since it has already been described in detail in the quoted papers, here we just mention that it is based on the observation that the major cost of each algorithm relies in the computation of the contrast modification function, i.e. the functions $R(x) = \sum_{y\in\mathfrak{I}} w(x,y)r(I(x), I(y))$ previously defined. The idea is then to perform a polynomial approximation of the functions r, separating their dependence on $I(x)$ and $I(y)$. Being the kernel w a function of $x-y$, the R-functions can then be expressed as suitable sums of convolutions between w and powers of I, which can be efficiently calculated through a Fast Fourier Transform (FFT), whose computational complexity is $\mathcal{O}(N \log N)$.

In practice this reduction of complexity means that we can use KBR and its anti-symmetric versions to process a high-resolution image in a matter of seconds instead of hours. Unlike most existing techniques to speed-up Retinex (see the Appendix, Sect. A.1) the procedure we apply significantly improves the time-performance without reducing the quality of the results nor modifying the essence of the algorithm in any way. Furthermore, we can choose the degree of the polynomial approximation so that our result does not deviate more than a given threshold from the result we would get without using the approximation (for details we refer the reader to Bertalmío et al. 2007).

We have implemented (38) and run it independently on all three channels of each color image. Each channel, originally in the range $[0, 255]$, has been normalized in the following way: adding 1 and dividing by 256, so the normalized value is in the range $[\frac{1}{256}, 1]$ and therefore we avoid divisions by zero. The set of parameters that correspond to the best visual performance varies with the input images; again, a precise parameter tuning is outside the scope of this paper, so in this section we fix values for the parameters that give overall good performances and we filter images with

Fig. 12 *Top left*: original image. *Top right*: output of path-wise Retinex with 20 Brownian paths per pixel. *Bottom left*: output of RSR with 20 sprays per pixel. *Bottom right*: output of Kernel Based Retinex (see text for details)

them. We have used this set of parameters: non-linear scaling function $f(r) = A\log(r) + 1$, $A = \frac{1}{\log(256)}$, normalized kernel $w(x, y) = \frac{\kappa}{w_0 + \|x-y\|}$ (where κ is a normalization constant, $w_0 = 0.1$ and $\|x - y\|$ denotes the Euclidean distance between pixels x and y), time step $\Delta t = 0.1$ and $\lambda = 3$ (for dark images, like the bottom one in Fig. 13 we use a smaller attachment to original data value: $\lambda = 2.5$). The stopping condition was determined by the difference between two consecutive iterations: if this is smaller than 0.25% in each of the three channels, then the process is stopped (usually convergence is achieved within 15–25 iterations). With the aforementioned speed-up scheme the whole processing time varies from 1 to 3 seconds for a 400×300 RGB image with a 3 GHz processor.

In Fig. 12 we compare the output of KBR with two other implementations of Retinex: Brownian paths and RSR (see Marini and Rizzi 2000 for details about the Brownian path implementation). We see that the output of our algorithm is free from halo artifacts and noise. Figure 13 shows the action of KBR and two other Retinex implementations, namely the ones presented in Jobson et al. (1997a) and Funt et al. (2004), obtained on a set of images suffering from different problems: lack of contrast, color cast, under-exposure. A proper comparison of these Retinex implementations is beyond the purpose of this paper and matter of further research. In Fig. 14 we can see the effect of changing the effective width w_0 of the kernel function $w(x, y)$, as well as a comparison with the output obtained with the anti-symmetrized KBR of (46) (which, as we mentioned, corresponds to iterating the ACE color correction algorithm (Rizzi et al. 2003; Bertalmío et al. 2007; Palma-Amestoy et al. 2009). Notice how the overexposed regions become even brighter with KBR, regardless of the kernel width, while with ACE the contrast is enhanced also in bright regions and details are not lost (shadows on the ground, tree leaves in the upper midregion of the picture.) Finally, Fig. 15 compares the output of KBR (38), anti-symmetrized KBR (46) and one of the *contrast decreasing* anti-symmetrizations of KBR, precisely $\mathcal{L}^{-F_2}(x) = \frac{1}{2} + \frac{1}{2}\delta C_w^{\min-\max}(I)(x)$. Notice how the results are as expected: KBR is not able to increase contrast on bright areas (like the white jacket on the boy at the bottom-left side of the picture), anti-symmetrized KBR performs well both on dark and bright areas, and the contrast decreasing anti-symmetrization of KBR does indeed decrease contrast (its output looks hazy, very much like photographs taken with a softening filter).

Fig. 13 For every image, *first row*: original picture (*left*) and output of KBR (*right*); *second row*: output of the Retinex implementations presented in Jobson et al. (1997a) (*left*) and in Funt et al. (2004) (*right*)

7 Conclusions

In this work we have provided a new interpretation of the Retinex theory, proposing an algorithm which complies with all the basic postulates of the Retinex theory. This method is based on the computation of the conditional expectation of a random variable in a density field generated by a ker-

Fig. 14 *Top left*: original image. *Top right*: output of KBR, kernel with $w_0 = 10$. *Bottom left*: output of KBR, kernel with $w_0 = 0.1$. *Bottom right*: output of anti-symmetrized KBR (46) (corresponding to ACE)

Fig. 15 *Top left*: original image. *Top right*: output of KBR. *Bottom left*: output of anti-symmetrized KBR (46). *Bottom right*: output of the *contrast decreasing* anti-symmetrized KBR discussed in the text

nel function, hence the name Kernel-Based Retinex, KBR for short. The KBR formulation has several advantages with respect to the original one: on the performance side, the computational complexity of KBR can be reduced from $\mathcal{O}(N^2)$ (which is the complexity of the original Retinex) to $\mathcal{O}(N \log N)$, thus permitting a considerable time saving; moreover it is not affected by the typical problems related to paths (or other structures with fixed geometry) such as noise, artifacts or haloes.

However, just like the original Retinex algorithm, KBR can only raise up the intensity of a pixel, thus it is unable to enhance over-exposed images and it is not idempotent. Comparing the KBR equation with those appearing in the variational framework introduced in (Palma-Amestoy et al. 2009) to perform perceptually-inspired color correction, we put in evidence that the sign of the first term in KBR is not the correct one to enhance contrast. On the contrary, the variational contrast lightness increases contrast and is able to deal both with under and over-exposed pictures.

We have also shown that the anti-symmetrization of the second term of KBR happens to coincide with an existing color perception algorithm called ACE (Rizzi et al. 2003; Bertalmío et al. 2007). This explicit relation between the Retinex theory and ACE, in the authors' opinion, clarifies the link among these two models, an issue which has been matter of research in recent years (Rizzi et al. 2004; Provenzi et al. 2008; Palma-Amestoy et al. 2009).

Finally, we have introduced an attachment to data term in KBR and its anti-symmetric versions. The corresponding algorithms converge to a non-trivial fixed point image.

Acknowledgements M. Bertalmío and V. Caselles acknowledge partial support by PNPGC project, reference MTM2006-14836, and IP-RACINE Project IST-511316. Edoardo Provenzi acknowledges the Ramón y Cajal fellowship by Ministerio de Ciencia y Tecnología de España.

Appendix

A.1 Overview on Different Retinex Implementations

As already stated, throughout this article we reserved the name Retinex to the original algorithm of Land and McCann (1971). Here we present a brief description of various implementations that followed the original one, in order to be acquainted both with significative refinements of the original model and with other formulations that were inspired by it. For an exhaustive description of all these algorithms see the quoted references. To put in evidence the fact that KBR is a coherent two-dimensional interpretation of the original Retinex model, we will divide this brief overview in two parts: firstly, we will discuss one-dimensional algorithms and then we will focus on two-dimensional Retinex versions. The terms one and two-dimensional refer to the sampling structures used to implement the Retinex algorithm.

One-dimensional implementations rely on the use of monodimensional geometrical structures such as paths in order to scan the image content. They are faithful to the original model, showing local White Patch (WP) properties. The major difference between them is the path geometry used: Land and McCann (1971) originally used piecewise linear paths, a geometry suggested by the Mondrian pictures. However, for general natural images, many piecewise linear paths are required to produce a noise-free output, and this affects the filtering time. To overcome this problem, in Cooper and Baqai (2004) and in Marini and Rizzi (2000), piecewise linear paths were substituted by more computationally efficient ones: double spirals and Brownian paths, respectively. Finally, there are multilevel one-dimensional Retinex implementations based on the work of Frankle and McCann (1983), further refined in Funt et al. (2004). The idea at the base of these algorithms is the following: the input image is progressively sub-sampled by averaging a number of pixels that grows as increasing powers of 2, on each sub-sampled level a ratio-reset computation (without threshold) is iterated a certain number of times, from the coarsest level to the finest one. This number turns out to be a crucial image-dependent parameter of the algorithm. Because of the sub-sampling, as we go far away from the target pixel, we do not consider actual pixel values, but average values of macro-areas of increasing size.

Two-dimensional Retinex-like algorithms were pioneered by Horn (1974) who reformulated Retinex as a Poisson equation. Horn was the first to criticize the use of paths, pointing out the need of a two dimensional version of Retinex. However, the model he proposed cannot be considered a coherent two-dimensional continuous representation *of the original Retinex*, because the fundamental ratio-reset mechanism is bypassed. Other works in line with Horn's Retinex interpretation are Blake (1985), that refined Horn's results using more suitable boundary constraints and Kimmel et al. (2003), which embedded Horn's formulation of Retinex in a variational setting.

Another type of two-dimensional Retinex-like version was proposed by Land himself in Land (1986), where, with a suitable modification of his original formulation, he noticed the possibility to reproduce Mach bands generated by a spinning white square on a black background. More precisely, he proposed to compute the lightness of the generic image pixel x as the logarithm of the ratio between its intensity $I(x)$ and *the average value of the surround*, sampled with a density that decays as the inverse of the square distance from the center. Thus, if we denote with L^{CS} this 'center/surround lightness', we have

$$L^{\mathrm{CS}}(x) = \log\left(\frac{I(x)}{\langle\{I(y),\, y \in \text{Surround}\}\rangle_w}\right), \tag{52}$$

where $\langle\cdot\rangle_w$ represents the weighted average operator. Comparing (52) with (1), it can be seen that there is a fundamental difference between this formulation and the original one, where the ratio is performed over the pixel with highest intensity and *not* over a weighted average value of the surround. In 1997, Jobson et al. (1997b) proposed a continuous version of Land's idea: they computed the weighted average of the surround by convolving the image function I with a normalized kernel function F (in the quoted paper they used a Gaussian). Using again the symbol L^{CS} for simplicity, we can represent this continuous center/surround lightness as:

$$L^{\mathrm{CS}}(x) = \log\left(\frac{I(x)}{(F * I)(x)}\right). \tag{53}$$

To overcome halo problems, the same authors refined their model proposing a multilevel approach (Jobson et al. 1997a), considering several convolutions with Gaussian functions with different standard deviations.

In more recent years, Provenzi et al. (2005, 2007) studied the basic mathematical properties of the original Retinex function, observed the redundancy implicit in the path formulation, and concluded in favor of the two-dimensional structure of random spray, as mentioned in Sect. 2.4 where we presented the RSR implementation.

Finally, inspired by the variational formulations of the contrast enhancement problem in Bertalmío et al. (2007), Palma-Amestoy et al. (2009), we reformulated the original principles of Retinex theory and proposed a coherent two-dimensional implementation of them. For that, at each

pixel x, we used an averaged ratio comparison between the channel color intensity at x and at a generic pixel y running over the entire image, avoiding the noise problems related to random sampling. We observed that, while the contrast enhancement models in Bertalmío et al. (2007); Palma-Amestoy et al. (2009) treat over and under-exposure in a symmetric way, Retinex (including our KBR formulation) does not correct over-exposed images. Mathematically, this is reflected in the anti-symmetric character of the contrast enhancement operators. We have shown that the anti-symmetrization of one of the terms of KBR leads us to ACE, which is a particular case of contrast enhancement operator, and the anti-symmetrization of the other term leads us to an operator that reduces contrast according to our formulation in Palma-Amestoy et al. (2009). This gives a clear picture of KBR and its similarities and differences with ACE and with the variational color correction algorithms described in Palma-Amestoy et al. (2009).

A.2 The First Variation of Contrast Functionals

Propositions 1 and 2 in the text were proved in Palma-Amestoy et al. (2009) and we omit here their proof. We just state and prove the general differentiation Lemma from which follow both Propositions.

Lemma 1 *Let $w : \mathfrak{I}^2 \to \mathbb{R}$ be a symmetric function in (x, y) and $S : (0, 1]^2 \to \mathbb{R}$ be a differentiable function in its variables (a, b). Let $S_1(a, b) = \frac{\partial S}{\partial a}(a, b)$. Then, given*

$$E(I) = \iint_{\mathfrak{I}^2} w(x, y) S(I(x), I(y))\, dx\, dy, \tag{54}$$

its first variation can be written as

$$\delta E(I) = 2 \int_{\mathfrak{I}} w(x, y) S_1(I(x), I(y))\, dy. \tag{55}$$

Proof Let $S_2(a, b) = \frac{\partial S}{\partial b}(a, b)$. Since $S(a, b) = S(b, a)$, for all $a, b > 0$, we have

$$S_1(a, b) = S_2(b, a). \tag{56}$$

By definition, the first variation of $E(I)$ in the direction δI is

$$\begin{aligned}\delta E(I, \delta I) = &\iint_{\mathfrak{I}^2} w(x, y) S_1(I(x), I(y)) \delta I(x)\, dx\, dy \\ &+ \iint_{\mathfrak{I}^2} w(x, y) S_2(I(x), I(y)) \delta I(y)\, dx\, dy.\end{aligned}$$

Interchanging the role of x and y in the second integral of the equation above and using (56) we get

$$\iint_{\mathfrak{I}^2} w(x, y) S_2(I(y), I(x)) \delta I(x)\, dx\, dy$$

$$= \iint_{\mathfrak{I}^2} w(x, y) S_1(I(x), I(y)) \delta I(x)\, dx\, dy \tag{57}$$

so that

$$\delta E(I, \delta I) = \int_{\mathfrak{I}} \left(2 \int_{\mathfrak{I}} w(x, y) S_1(I(x), I(y)) \right) \delta I(x)\, dx \tag{58}$$

and the proposition follows. □

References

Ambrosio, L., Gigli, N., & Savaré, G. (2005). Gradient flows in metric spaces and in the space of probability measures. In Lectures in mathematics, Basel: Birkhäuser.

Barash, D. (2002). A fundamental relationship between bilateral filtering, adaptive smoothing, and the nonlinear diffusion equation. *IEEE Transactions on Pattern Analysis and Machine Intelligence*, *24*, 844–847.

Bertalmío, M., & Cowan, J. (2009). Implementing the Retinex algorithm with Wilson-Cowan equations, *Journal of Physiology, Paris* (to appear).

Bertalmío, M., Caselles, V., Provenzi, E., & Rizzi, A. (2007). Perceptual color correction through variational techniques. *IEEE Transactions on Image Processing*, *16*, 1058–1072.

Blake, A. (1985). Boundary conditions of lightness computation in Mondrian world. *Computer Vision, Graphics and Image Processing*, *32*, 314–327.

Bressloff, P., Cowan, J., Golubitsky, M., Thomas, P., & Wiener, M. (2002). What geometric visual hallucinations tell us about the visual cortex. *Neural Computation*, *14*(3), 473–491.

Cooper, T. J., & Baqai, F. A. (2004). Analysis and extensions of the Frankle-McCann Retinex algorithm. *Journal of Electronic Imaging*, *13*, 85–92.

Frankle, J., & McCann, J. J. (1983). Method and apparatus for lightness imaging. U.S. Patent, 4, 348,336, 1983.

Funt, B., Ciurea, F., & McCann, J. J. (2004). Retinex in MATLAB. *Journal of Electronic Imaging*, *13*(1), 48–57.

Glasser, L., McKinney, A., Reilly, C., & Schnelle, P. (1958). Cube-root color coordinate system. *Journal of the Optical Society of America*, *48*, 736–740.

Horn, B. (1974). Determining lightness from an image. *Computer Graphics and Image Processing*, *3*, 277–299.

Hurlbert, A. (1986). Formal connections between lightness algorithms. *Journal of the Optical Society of America A*, *3*, 1684–1693.

Jobson, D., Rahman, Z., & Woodell, G. (1997a). A multiscale Retinex for bridging the gap between color images and the human observation of scenes. *IEEE Transactions on Image Processing*, *6*(7), 965–976.

Jobson, D., Rahman, Z., & Woodell, G. (1997b). Properties and performance of a center/surround Retinex. *IEEE Transactions on Image Processing*, *6*(3), 451–462.

Kimmel, R., Elad, M., Shaked, D., Keshet, R., & Sobel, I. (2003). A variational framework for Retinex. *International Journal of Computer Vision*, *52*, 7–23.

Land, E. (1977). The Retinex theory of color vision. *Scientific American*, *237*, 108–128.

Land, E. (1983). Recent advances in Retinex theory and some implications for cortical computations: Color vision and the natural image. *Proceedings of the National Academy Science of the United State of America*, *80*, 5163–5169.

Land, E. (1986). An alternative technique for the computation of the designator in the Retinex theory of color vision. *Proceedings of the National Academy Science of the United State of America*, *83*, 3078–3080.

Land, E., McCann, J. (1971). Lightness and Retinex theory. *Journal of the Optical Society of America*, *61*(1), 1–11.

Marini, D., & Rizzi, A. (2000). A computational approach to color adaptation effects. *Image and Vision Computing*, *18*, 1005–1014.

Marr, D. (1974). The computation of lightness by the primate retina. *Vision Research*, *14*(12), 1377–1388.

McCann, J., McKee, S., & Taylor, T. (1976). Quantitative studies in Retinex theory: a comparison between theoretical predictions and observer responses to the 'color mondrian' experiments. *Journal of Vision Research*, *16*, 445–458.

McCann, J. J. (2004). Capturing a black cat in shade: past and present of Retinex color appearance models. *Journal of Electronic Imaging*, *13*(1), 36–47.

Palma-Amestoy, R., Provenzi, E., Caselles, V., & Bertalmío, M. (2009). A perceptually inspired variational framework for color enhancement. *IEEE Transactions on Pattern Analysis and Machine Intelligence 31*(3), 458–474.

Provenzi, E., De Carli, L., Rizzi, A., & Marini, D. (2005). Mathematical definition and analysis of the Retinex algorithm. *Journal of the Optical Society of America A*, *22*(12), 2613–2621.

Provenzi, E., Fierro, M., Rizzi, A., De Carli, L., Gadia, D., Marini, D. (2007). Random spray Retinex: a new Retinex implementation to investigate the local properties of the model. *IEEE Transactions on Image Processing*, *16*, 162–171.

Provenzi, E., Gatta, C., Fierro, M., & Rizzi, A. (2008). A spatially variant white patch and gray world method for color image enhancement driven by local contrast. *IEEE Transactions on Pattern Analysis and Machine Intelligence 30*(10), 1757–1770.

Rizzi, A., Gatta, C., & Marini, D. (2003). A new algorithm for unsupervised global and local color correction. *Pattern Recognition Letters*, *24*, 1663–1677.

Rizzi, A., Gatta, C., & Marini, D. (2004). From Retinex to automatic color equalization: issues in developing a new algorithm for unsupervised color equalization. *Journal of Electronic Imaging*, *13*(1), 75–84.

Tomasi, C., & Manduchi, R. (1998). Bilateral filtering for gray and color images. In *ICCV '98: Proceedings of the sixth international conference on computer vision*, Washington, DC, USA, 1998 (pp. 839–846). IEEE Computer Society, Los Alamitos.

Wilson, H., & Cowan, J. (1972). Excitatory and inhibitory interactions in localized populations of model neurons. *Biophysical Journal*, *12*, 1–24.

Wilson, H., & Cowan, J. (1973). A mathematical theory of the functional dynamics of cortical and thalamic nervous tissue. *Biological Cybernetics*, *13*(2), 55–80.